GAS TECHNOLOGY

The Effect of Water Influx on p/z-Cumulative Gas Production Curves

J. R. BRUNS
MEMBER AIME
M. J. FETKOVICH
JUNIOR MEMBER AIME
V. C. MEITZEN

PHILLIPS PETROLEUM CO.
BARTLESVILLE, OKLA.

Abstract

The relationship between p/z and cumulative gas production for typical gas reservoirs was studied by calculating pressure response to various modes of gas production and water encroachment. Water encroachment methods considered were Schilthuis, Hurst simplified and van Everdingen-Hurst. In the method, the assumptions normally made in water encroachment calculations were accepted. Normally, pressures are measured and the gas reserves and water encroachment found implicitly. Conversely, in this work various encroachment factors, reserves and reservoir-aquifer geometry were assumed and the pressures solved implicitly.

The results show the spectrum of p/z shapes that can be expected for real reservoirs. With normal encroachment rates for closed aquifers the p/z chart exhibits the typical inflection at early times. This has sometimes been interpreted as all measurement error. These studies have shown that a new look should be taken at interpretation. It is rather dangerous to extrapolate "straight-line" p/z charts if encroachment from an aquifer is suspected.

Introduction

A common method of predicting gas reserves is the graphical solution to the gas material balance equation. A special case of the material balance equation is linear in p/z with cumulative gas production (G_p) which predicts the initial in-place gas when p/z is extrapolated to zero. Derivation of this form is based on the equation of state, corrected for compressibility ($pV = znRT$), and, particularly, on the reservoir being closed (no water encroachment). A straight line on the p/z chart results when these conditions hold. However, an apparent straight line on the chart does not assure that the reservoir is closed. Many of the curves show a rapid decline in the early stages of production after which they flatten out. Confusion arises as to whether these characteristics are caused totally by pressure measurements. To answer this question in part, a series of controlled mathematical experiments was performed in which a typical gas field was produced subject to various forms of water encroachment. These runs were specifically designed to eliminate measurement errors by calculating pressures at the inner boundary of the aquifer. The resultant p/z charts were thus made available for study and direction in predicting reserves and to indicate the curvature that can be expected in addition to that caused by normal measurement error.

Original manuscript received in Society of Petroleum Engineers office July 13, 1964. Revised manuscript received Feb. 2, 1965. Paper presented at SPE 39th Annual Fall Meeting held in Houston, Tex., Oct. 11-14, 1964.

Solution of the Basic Equation for p/z

The basic equation solved for p and p/z is derived in Appendix A. It is

$$G_a = G_r + \frac{K.S(p,t)}{B_g - B_{gi}} \quad \ldots\ldots\ldots \quad (1)$$

G_a and G_r are the apparent and real values of original gas in place and are derived by assuming a closed reservoir for G_a, and one open to an aquifer for G_r. The function $S(p,t)$ is defined by three methods—Schilthuis, Hurst simplified or van Everdingen-Hurst.[1-4] The definitions of these functions are given in Appendix B.

Eq. 1 is the linear function that is commonly plotted (G_a vs $S(p,t)/B-B_i$) with the intercept predicting the original gas in place and slope predicting the water encroachment factor.[3,4] This is a graphical solution of Eq. 1 when histories on pressure and cumulative productions are known. In some cases the equation has been rearranged so a plot can be made such that the encroachment factor is predicted by the intercept and the reserve by the slope.[3]

In the calculations presented in this paper, in-place values, water encroachment factors, rock fluid properties, and cumulative production were set. Eq. 1 was solved implicitly for p/z.

The equivalent of Eq. 1 in terms of p/z is

$$p/z = \frac{p_i}{z_i}\left[\frac{G_r - G_p}{G_r - \frac{z_i T p_{sc}}{T_{sc} p_i K.S(p,t)}}\right] \quad \ldots \quad (2)$$

[1]References given at end of paper.

Setting $K_e S(p,t) = 0$ (no water encroachment), produces the linear form. Obviously, whether the p/z curve is linear or not when $K_e S(p,t) \neq 0$ depends upon the $S(p,t)$ function.

The cumulative productions were determined from production rates calculated from wellhead operating curves subject to the maximum allowables.[3] The wellhead curve is defined by

$$q_g = C(p_{wh}^2 - p_{tf}^2)^n. \quad \ldots\ldots\ldots \quad (3)$$

where q_g = the production rate, Mscf/D
C = the performance coefficient
p_{wh} = the wellhead shut-in pressure, psia
p_{tf} = the tubing flowing pressure
n = the back-pressure exponent.

Shut-in wellhead pressures were determined after the reservoir pressure p was chosen by calculating the static head by the method of Cullender and Smith.[4] The static head was subtracted from p to give p_{wh}.

A general flow scheme of the calculation technique is given in Fig. 1, and the field conditions are given in Table 1.

Compressibilities were interpolated from the 1952 API tables. Tables 2 and 3 list conditions that were varied for individual runs.

Discussion of Results

The results of the calculations are shown in Figs. 2 through 9. All of the curves show p/z as a function of cumulative gas produced and are labeled with the numbers corresponding to the data in Tables 2 and 3. Each plotted point represents two years.

Fig. 2 gives the results when the aquifer was assumed to be unlimited, or when original aquifer pressure was assumed to remain constant at some outer boundary (Schilthuis). As the encroachment factor was increased the pressure was maintained at a higher and higher level. The dotted line at the bottom represents no encroachment and the top dotted line shows complete pressure maintenance by a very active water drive.

Fig. 3 shows the results of increasing the Hurst simplified encroachment factor from 2.5×10^4 to 2.5×10^6 (cu ft) ln (mo)/psi/year.

The van Everdingen-Hurst encroachment factors were assumed for runs shown in Figs. 4 through 9, and the aquifer was assumed closed and radial. Combinations of three variations in relative aquifer size, two water compressibilities and nine aquifer permeabilities were represented in the runs.

Curves with inflections, which have been observed in practice, were produced for the closed aquifers.

In most cases the families of curves appear to approach a common slope at zero time. At zero time this slope will represent the p/z line for no water encroachment.

Runs with the Schilthuis method and Hurst-simplified method converge at or near a horizontal line as water encroachment factors increase. This means that pressure drops in the aquifer are approaching zero.

In the van Everdingen-Hurst runs the curves respond to the mobility (k/μ) and compressibility of the water, and the relative size of the aquifer. For R_e/R_r of 1.5.

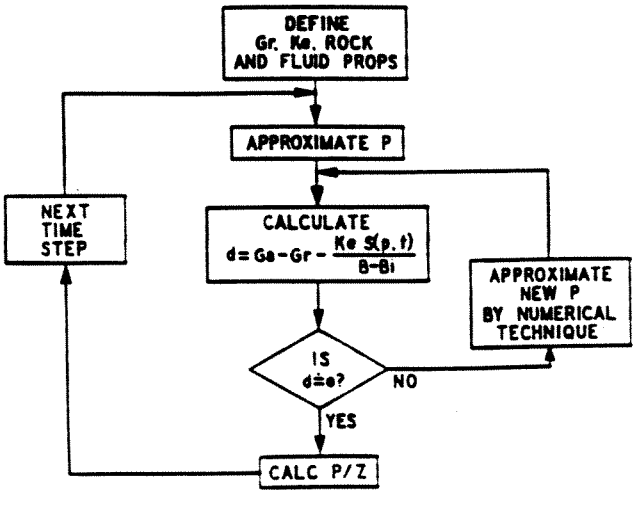

Fig. 1—Solution of Eq. A-12 for p/z.

TABLE 1—FIELD CONDITIONS

Area = 2,500 acres
Pay = 100 ft
Porosity = 0.25
Connate water = 0.3
Original BHP = 5,000 psia
Formation temperature = 250F
Depth = 10,000 ft
Gas Gravity = 0.68 (No N_2, CO_2 or H_2S)
$(\text{Radius})^2 = 34.7\times10^6$ sq ft
Initial wellhead shut-in pressure = 4,200 psia
Wellhead shut-in temperature = 100F
Back-pressure curve slope = 0.7
Open flow potential = 74.4 MM scf/D
Minimum wellhead flowing pressure = 100 psia
Maximum allowable field rate = 47.2 MM scf/D

TABLE 2—VARIABLE CONDITIONS FOR RUNS 1 THROUGH 14

Run No.	Type Encroachment Factor	Encroachment Factor
1	↑	5,900
2		18,000
3	Schilthuis	36,000
4	(cu ft/psi/year)	59,000
5	Radial Infinite	100,000
6		200,000
7	↓	590,000
8	↑	25,000
9		90,000
10	Hurst Simplified	150,000
11	(cu ft ln (month)/psi/year)	250,000
12	Radial Infinite	340,000
13		610,000
14	↓	2,500,000

TABLE 3—VARIABLE CONDITIONS FOR RUNS 15 THROUGH 38

Run No.	Type Encroachment Factor	Ratio of Aquifer Radius to Field Radius	Aquifer Permeability (md)	Dimensionless Time to Real Time Ratio (1/year)	Water Compressibility (1/psi)
15		1.5	1	.089	3.0×10^{-6}
16		1.5	10	.89	3.0×10^{-6}
17	↓	1.5	100	8.9	3.0×10^{-6}
18		5.0	1	.089	3.0×10^{-6}
19	van Everdingen	5.0	10	.89	3.0×10^{-6}
20	Hurst Radial Finite	5.0	100	8.9	3.0×10^{-6}
21	16,350 cu ft/psi	5.0	1000	89.	3.0×10^{-6}
22		10.0	1	.089	3.0×10^{-6}
23		10.0	10	.89	3.0×10^{-6}
24		10.0	100	8.9	3.0×10^{-6}
25	↓	10.0	1000	89.	3.0×10^{-6}
26		10.0	10000	890.	3.0×10^{-6}
27		1.5	10	.089	30×10^{-6}
28		1.5	100	.89	30×10^{-6}
29	↓	5.0	10	.089	30×10^{-6}
30		5.0	18	.16	30×10^{-6}
31	van Everdingen	5.0	39.3	.35	30×10^{-6}
32	Hurst Radial Finite	5.0	100	.89	30×10^{-6}
33	163,500 cu ft/psi	10.0	10	.089	30×10^{-6}
34		10.0	15.8	.141	30×10^{-6}
35		10.0	31.5	.28	30×10^{-6}
36		10.0	100	.89	30×10^{-6}
37	↓	10.0	1000	8.9	30×10^{-6}
38		10.0	10000	89.	30×10^{-6}

determined as 70.5 percent. The trapped gas saturation is therefore, 29.5 percent.

In the depletion test, the pressure at the outlet face was lowered from 218.8 to 58.0 psia [1.506 to 0.400 MPa]. Table 4 shows the pressure vs. the cumulative water production. From a pressure of 218.8 to about 188.5 psia[1.506 to 1.300 MPa], water was produced in conjunction with traces of gas. In the pressure range of 181.2 to 152.2 psia [1.249 to 1.049 MPa], mainly water was produced with some small gas production, then from 145.0 to 58.0 psia [1.000 to 0.400 MPa] gas was the dominant fluid produced. By the termination of the test the average water saturation was 49.2 percent.

In the third test (i.e., the reinjection test), water was injected at a rate of 0.35 cm^3/hr. As a result, gas began to be produced from the upper end that was kept at a constant pressure of 59.5 psia [0.410 MPa]. Gas production continued for a cumulative water injection of 19.9 cm^3, whereafter no gas was produced. The final water and gas saturations were determined as 62.3 and 37.7 percent, respectively. The third test, therefore, determines a mobilized gas saturation of 37.7 percent for Core A.

Core B - The first test for Core B started with an initial water saturation of 19.5 percent. The water injection rate was 0.35 cm^3/hr and the core outlet pressure was kept at 217.5 psia [1.500 MPa]. After a cumulative injection of 92.28 cm^3, water breakthrough was observed. No gas production was observed after the water breakthrough. Water saturation at the end of the first test was 68.9 percent, and therefore the trapped gas saturation was 31.1 percent.

The depletion test for Core B showed a production pattern similar to that of Core A. From a pressure of 217.5 to 195.7 psia [1.500 to 1.349 MPa], water in conjunction with a trace amount of gas was produced, then down to a pressure of about 174.0 psia [1.200 MPa], low gas production was accompanied by water production. In the pressure range of 166.7 to 145.0 psia [1.150 to 1.000 MPa] both gas and water phases were produced, followed by nearly all gas and little water production from 137.7 to 58.0 psia [0.849 to 0.400 MPa]. Table 5 lists core outlet pressure and cumulative water production for the depletion test. Average water and gas saturation measured at the end of the second test were 53.7 and 46.3 percent respectively.

In the third test water was injected at a constant rate of 0.37 cm^3/hr in the lower end of the core. Gas production began as a result of gas injection. During the course of injection, core outlet pressure was kept at 60.9 psia [420 kPa]. Gas production showed a piston-like behavior. Water breakthrough occurred after a cumulative injection of 9.70 cm^3 of water. The measured water and gas saturation by the end of the third test were 59.0 and 41.0 percent, respectively.

Core C - This core was completely saturated with the gas, and then water was injected at a constant rate of 0.49 cm^3/hr and a core outlet pressure of 217.5 psia [1.500 MPa]. After a cumulative water injection of 148.2 cm^3, water breakthrough was observed. Similar to experiments on Cores A and B, no further gas production was observed after the breakthrough. The trapped gas saturation was determined to be 28.0 percent for Core C.

In the depletion test, the core pressure was lowered from 216.2 to 50.5 psia [1.490 to 0.348 MPa]. From a pressure of 216.2 to 181.2 psia [1.490 to 1.249 MPa], only water was produced, later on gas and water production followed a pattern similar to depletion tests for Cores A and B. At the termination of the test, the measured water and gas saturations were 52.9 and 47.1 percent, respectively. Table 6 gives the pressure and cumulative water production history and average water saturation for this test.

In the reinjection test, water was injected at a rate of 0.49 cm^3/hr with a core outlet pressure of 50.5 psia [348 kPa]. For a cumulative water injection rate of 12.3 cm^3, gas was produced at the top face. Injection of water did not produce any more gas after a water cumulative injection of 12.3 cm^3. The measured water and gas saturations at the termination of the third test were 58.9 and 41.1 percent, respectively.

NUMERICAL MODELLING OF LABORATORY EXPERIMENTS

Numerical modelling of the experiments described above was carried out to get an insight into the tests. For this purpose, a commercial model - Eclipse[12] was used. This model is a 3-D, three-phase reservoir simulator of the implicit-type. To simulate the tests, core length was divided into 40 equal grids. The simulation and the history matching process for Core C will be presented first.

The first test of water flooding the core does not require numerical simulation due to experimental evidence of piston-like displacement. We will simulate the depletion tests in the following.

The relative permeability functions used in simulating the second test has the form:[13]

$$k_{rw} = 0.3\ (S_w^*)^n \tag{1}$$

$$k_{rg} = 0.8\ (1-S_w^*)^n \tag{2}$$

where

$$S_w^* = \left[\frac{S_w - S_{wc}}{1 - S_{wc} - S_{gr}} \right] \tag{3}$$

In Eqs. 1 and 2 Corey exponent n is assumed to be 3. We also assume $S_w = 0.1$. Other parameters of the above equations are defined in the nomenclature. Fig. 2 shows the P_c vs. the water saturation. The expression for the relative permeabilities and the capillary pressure function are believed to be representative of the fluids/rock system of this study. In simulating the depletion test, residual gas saturation (i.e., S_{gr} of Eq. 3) was found to be the most sensitive parameter. Variation of the water relative permeability curve and the P_c function had an effect of less than the residual gas saturation. We used residual gas saturation of 28 percent as our first guess for the history matching. Fig. 3 shows the measured core outlet pressure and cumulative water production for the depletion test. The same figure also shows the simulated results for three different values of residual gas saturation. This figure indicates that if we assume the mobilized gas saturation to be identical to the initial trapped gas saturation of 28 percent, the pressure in the core will drop very rapidly. Assuming a mobilized gas saturation of 35 percent improves the history match of the depletion test. With a mobilized gas saturation of 41 percent, the match between the measured and simulated results for the pressure-cumulative water production history becomes excellent. It is interesting to note that the value of the mobilized gas saturation that is solely based on the history match of the second test is almost the same as the residual gas saturation measured from the third test. On the other hand, the average gas saturation measured from the second test is 47.1 percent. Fig. 4 explains the reason for this difference. This figure shows the saturation profiles along the core length for a residual gas saturation of 41 percent at various stages of depletion. Fig. 4a shows that after production of some 16.6 cm^3 of water, the saturation distribution along the core is uniform, with a gas saturation of about 36 percent. For this stage of depletion, the core outlet pressure from simulation is 166 psia [1.145 MPa], and no gas production is computed. After producing 28.8 cm^3 of water when the core outlet pressure is 138 psia [951 kPa], gas saturation varies along the core length (see Fig. 4b). In the top four simulation blocks, gas saturation is around 50 percent, for the bottom half of the blocks gas saturation is about 41 percent and for the remaining blocks it varies from 42 to 43 percent. Fig. 4c shows the gas saturation profile at a later stage of depletion where the simulated water production and core outlet pressure are 34.1 cm^3 and 107 psia [738 kPa], respectively. The gas saturation in this stage of depletion for the 5 top grid blocks varies from 50 to 57 percent. For most of other blocks gas saturation is around 41 to 42 percent. The gas saturation profile by the end of the depletion test is shown in Fig. 4d. For this last stage, gas saturation of the top 5 simulation blocks averages 60 percent while the gas saturation of the

bottom blocks is about 41 percent. Qualitatively, the gas saturation profiles of Fig. 4 indicate that gas saturation varies along the core length and therefore the average gas saturation established from the depletion test is higher than the mobilized gas saturation.

Fig. 5 shows the core outlet pressure vs. the cumulative gas production for Core C. This figure indicates that except in the early period of gas production, a good match between the measured data and the simulation results for a S_{gr} of 41 percent exists.

The depletion tests for Cores A and B were also simulated in the same manner as for Core C. Fig. 6 compares simulation of the depletion test and the measurements for Core A. Unlike Fig. 3 which shows a good match between measured data and simulation results, Fig. 6 does not show a close agreement. The best possible match which is shown in Fig. 6 is based on a residual gas saturation of 42 percent. The measured residual gas saturation for Core A from the reinjection test is 37.7 percent.

Fig. 7 compares the measured and simulated values of core outlet pressure and cumulative water production for Core B. The agreement between measured data and simulation results is excellent when a residual gas saturation of 41 percent is assumed. This value of residual gas saturation is identical to the value of the residual gas saturation measured from the reinjection test.

CONCLUSIONS

1. The effect of initial water saturation on the trapped gas saturation for the sands examined in this paper is small. The trapped gas saturation increases as the initial water saturation increases.
2. Two distinct values of residual gas saturation have been observed for the sands. The lower value corresponds to the initial entrapment, and the higher value to the gas saturation to be mobilized under expansion. These values for the sand of Table 3 are about 30 and 40 percent of pore volume, respectively.
3. The depletion test, when the trapped gas is expanded to be mobilized may provide an average gas saturation that is higher than the mobilized gas saturation. A reinjection test could provide proper value of the mobilized gas saturation. Numerical simulation of the depletion test could also assist in proper estimation of mobilized gas saturation.
4. An important consequence of the difference between the initial entrapped and final mobilized gas saturations is the delay of entrapped gas migration from the water invaded region to the gas zone. Both classic material balance relationships and simulation have to account for this.

NOMENCLATURE

k_{rw} = water relative permeability
k_{rg} = gas relative permeability
n = Corey exponent
P_c = capillary pressure
S_w = water saturation, fraction or percentage
S_g = gas saturation, fraction
S_{wc} = irreducible water saturation, fraction
S_{gr} = residual gas saturation, fraction or percentage

ACKNOWLEDGEMENT

The experimental phase of the research program was carried out by ResLab of Trondheim, Norway under the sponsorship of Norsk Hydro.

We thank Norsk Hydro for permission to publish this paper and Odd Hjelmeland of ResLab for the experimental runs. SUPRI-B Industrial Affiliates Program provided the financial support for writing this paper.

REFERENCES

1. Geffen, T. M., Parrish, D. R., Haynes, G. W., and Morse, R. A.: "Efficiency of Gas Displacement from Porous Media by Liquid Flooding", Trans., AIME (1952) **195**, 29-38.
2. Chierici, G. L.,, Ciucci, G. M., and Long, G.: "Experimental Research on Gas Saturation Behind the Water Front in Gas Reservoirs Subjected to Water Drive", Proc., Sixth World Pet. Cong., Frankfurt (1963) Sec. II/Paper 17-PD6, 483-498.
3. Keelan, D. K., and Dugh, V. J.: "Trapped-Gas Saturation in Carbonate Formations", Soc. Pet. Eng. J. (April 1975) 149-160.
4. Katz, D. L., et al.: "How Water Displaces Gas From Porous Media", Oil and Gas J. (Jan. 10, 1966) 55-60.
5. Agarwal, R. G., Al-Hussainy, R., and Ramey, H. J., Jr.: "The Importance of Water Influx in Gas Reservoirs", J. of Pet. Tech. (Nov. 1965) 1336-42.
6. Lutes, J. L., Chiang, C. P., Rossen, R. H., and Brady, M. M.: "Accelerated Blowdown of a Strong Water-Drive Gas Reservoir", J. of Pet. Tech. (Dec. 1977) 1533-1538.
7. Chesney, T. P., Lewis, R. C., and Trice, M. L.: "Secondary Gas Recovery From a Moderately Strong Water Drive Reservoir: A Case History", J. of Pet. Tech. (Sept. 1982) 2149-2157.
8. Boyd, W. E., Christian, L. D., and Danielsen, C. L.: "Secondary Gas Recovery From a Watered-Out Reservoir", SPE 11158, paper presented at the 57th Annual Fall Technical Conference and Exhibition, New Orleans, LA, Sept. 26-29, 1982.
9. Fishlock, T. P., Smith, R. A., Soper, B. M., and Wood R. W.: "Experimental Studies on the Waterflood Residual Gas Saturation and its Production by Blowdown", SPE 15455, paper presented at the 61st Annual Technical Conference and Exhibition of SPE, New Orleans, Oct. 5-8, 1986.
10. Olds, R. H., Sage, B. H., and Lacey, W. N.: "Phase Equilibrium in Hydrocarbon Systems-Composition of the Dew-Point Gas of the Methane-Water System", Ind. Eng. Chem. (Oct. 1942) 1223-27.
11. Culberson, O. L., and McKetta, J. J.: "Phase Equilibrium in Hydrocarbon-Water Systems,-III - The Solubility of Methane in Water at Pressures to 10,000 psia", Trans., AIME (1951) **192**, 223-26.
12. "Eclipse Reference Manual", Exploration Consultants Limited, Oxfordshire, England (1985).
13. Corey. A. T.: "The Interrelation Between Gas and Oil Relative Permeabilities", Producers Monthly, (Nov. 1954) 38-41.

Table 1 - RESIDUAL GAS SATURATION OF UNCONSOLIDATED AND CONSOLIDATED POROUS MEDIA OF CHIERICI, et al.[2]

	Unconsolidated Samples				Sandstone Samples			
Core Designation	A	B	C	D	a	b	c	d
Diameter, cm	11.1	11.1	11.1	11.1	10.0	10.0	10.0	10.0
Length, cm	27.4	28.3	25.5	25.5	22.6	26.0	22.1	18.8
Porosity, %PV	49.4	32.8	32.8	34.9	20.7	18.9	22.1	21.2
Permeability, md	6,170	3,710	12,140	12,950	160.2	63.1	112.6	91.3
Irreducible Water Saturation, %PV	26.5	21.5	23.8	19.0	35.5	40.0	33.5	37.0
Flooding Pressure, psia	3,000	2,886	2,886	2,915	2,872	2,900	2,915	2,872
S_{gr} at Flooding Pressure, %PV	19.5	22.3	24.5	21.6	43.8	38.7	38.9	34.8
S_{gr} at the end of Depletion, %PV	32.6	24.3	27.5	37.4	42.1	42.8	40.9	37.8

Table 2 - RESIDUAL GAS SATURATION MEASUREMENTS OF FISHLOCK, et al.[9]

	High Permeability Core	Low Permeability Core
Diameter, cm	4.5	4.5
Lenth, cm	167.6	84.1
Porosity, %PV	20.0	11.6
Permeability, md	1280	240
Irreducible Water Saturation, %PV	-	-
Flooding Pressure, psia	3,960	4,075
S_{gr} at Flooding Pressure, %PV	35.4	41.5
S_{gr} at the end of Depletion, %PV	49	45.5

Table 3 - CORE DIMENSIONS AND PROPERTIES OF THIS STUDY

Core	Length, cm	Diameter, cm	Porosity, %PV	Pemeability, md
A	45.00	3.75	34.9	1,915
B	50.95	3.75	33.2	1,445
C	54.25	3.75	34.4	1,792

Table 4 - EXPERIMENTAL DATA OF PRESSURE DEPLETION TEST FOR CORE A

Core Outlet Pressure, psia	Cumulative Water Production, cm^3	Average S_w, %
218.8	0.0	70.5
210.5	2.42	69.1
203.0	4.85	67.7
195.7	7.28	66.3
188.5	9.88	64.8
181.2	12.65	63.2
174.7	15.43	61.6
166.7	18.20	60.0
159.5	21.32	58.2
152.2	24.27	56.5
145.0	26.00	55.5
138.0	27.91	54.4
130.6	28.10	54.3
123.2	28.10	54.3
116.0	28.10	54.3
101.5	28.25	54.2
87.3	31.20	52.5
72.6	31.90	52.1
58.0	34.15	50.8

Table 5 - EXPERIMENTAL DATA OF PRESSURE DEPLETION TEST FOR CORE B

Pressure, psia	Cumulative Water Production, cm^3	Average S_w, %
216.5	0.	68.9
210.4	2.25	67.7
201.8	4.67	66.4
195.7	6.35	65.5
187.6	8.59	64.3
181.3	10.84	63.1
172.4	14.01	61.4
166.7	16.44	60.1
159.4	19.05	58.7
152.4	22.60	56.8
145.0	24.09	56.0
137.7	24.09	56.0
130.5	24.46	55.8
123.3	25.40	55.3
116.0	25.59	55.2
107.6	25.59	55.2
101.5	25.76	55.1
87.0	26.71	54.6
72.5	28.39	53.7
58.0	28.39	53.7

Table 6 - EXPERIMENTAL DATA OF PRESSURE DEPLETION TEST FOR CORE C

Core Outlet Pressure, psia	Cumulative Water Production, cm^3	Average S_w, %
216.2	0.	72.0
203.0	3.10	70.5
195.7	5.56	69.3
188.5	7.83	68.2
181.2	10.30	67.0
173.4	13.40	65.5
166.6	16.08	64.2
159.5	18.97	62.8
152.2	22.27	61.2
145.0	24.7	60.0
137.5	27.00	58.9
130.5	30.09	57.4
123.8	32.77	56.1
116.0	32.77	56.1
107.9	33.39	55.8
101.6	35.66	54.7
85.4	35.87	54.6
69.6	39.37	52.9
50.5	39.37	52.9

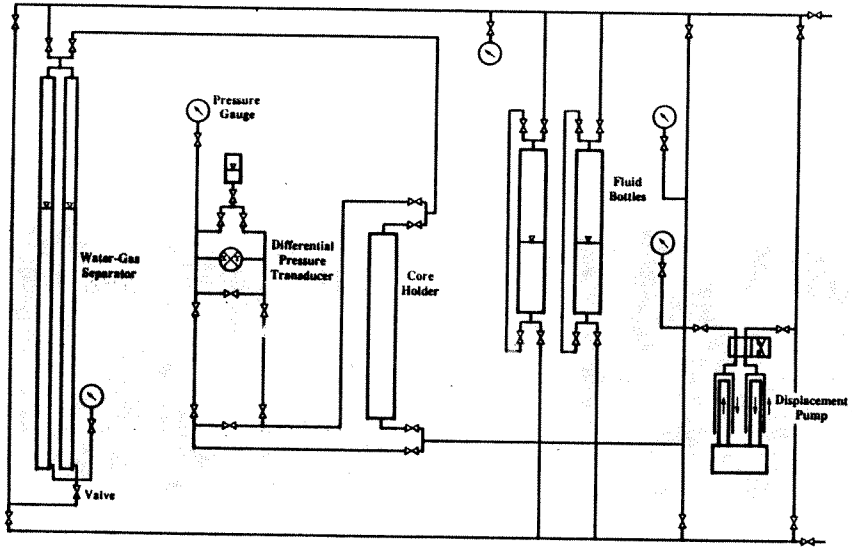

Fig. 1—Schematic of experimental apparatus.

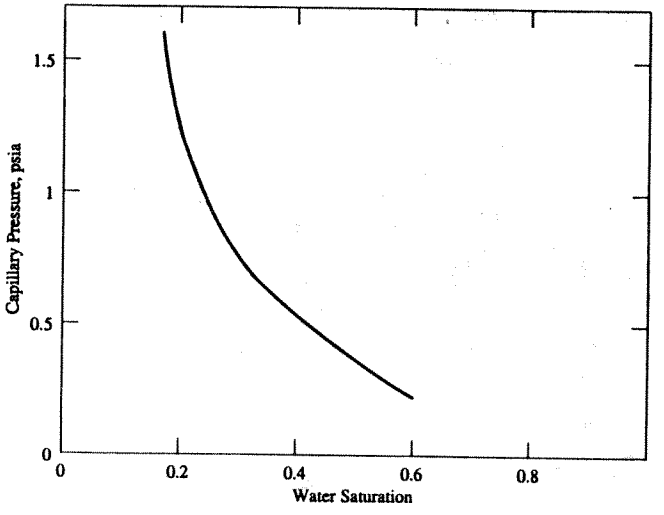

Fig. 2—Capillary pressure curve used in the simulation of the depletion tests.

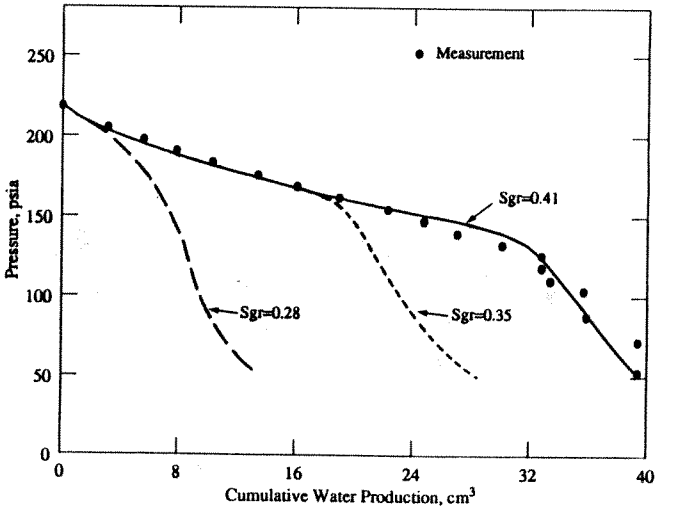

Fig. 3—History matching of Core C outlet pressure vs. cumulative water production of the depletion test.

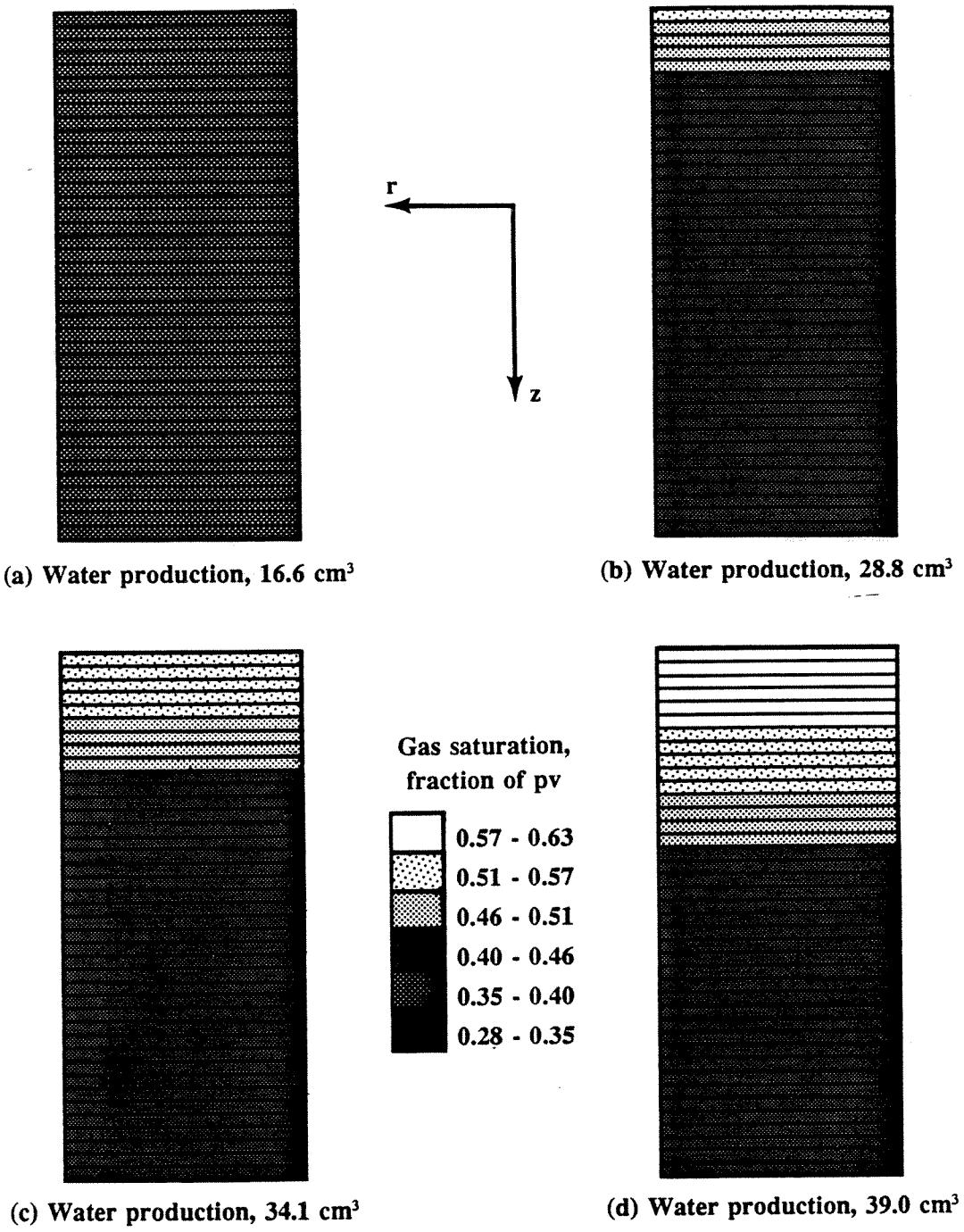

(a) Water production, 16.6 cm³

(b) Water production, 28.8 cm³

(c) Water production, 34.1 cm³

(d) Water production, 39.0 cm³

Fig. 4—Simulated gas saturation profiles at various stages of depletion of Core C.

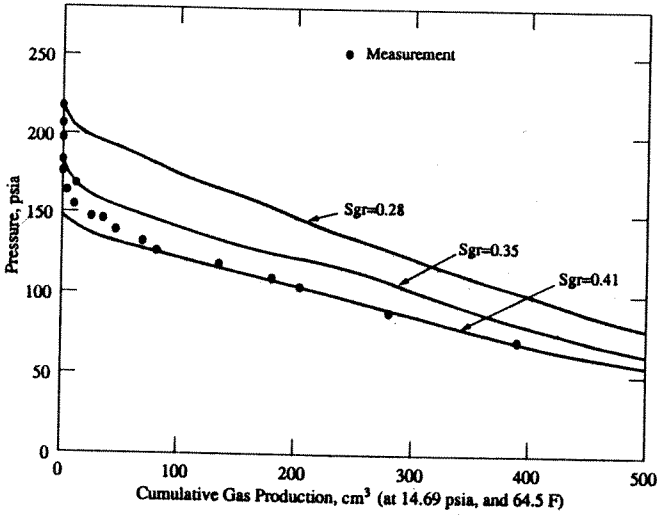

Fig. 5—History matching of Core C outlet pressure vs. cumulative gas production of the depletion test.

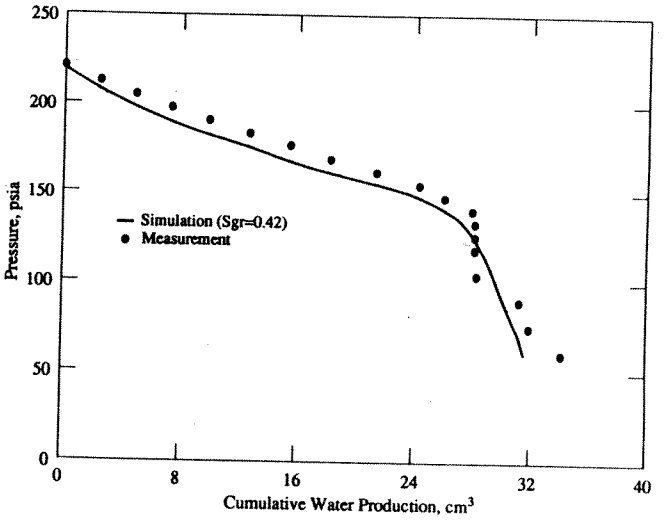

Fig. 6—History matching of Core A outlet pressure vs. cumulative water production of the depletion test.

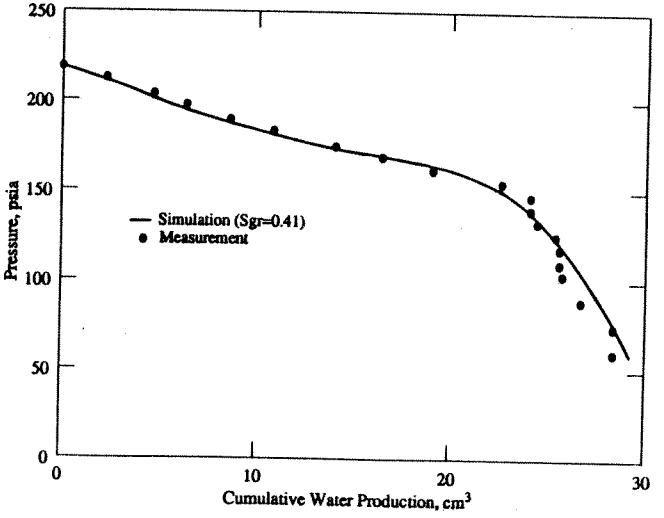

Fig. 7—History matching of Core B outlet pressure vs. cumulative water production of the depletion test.

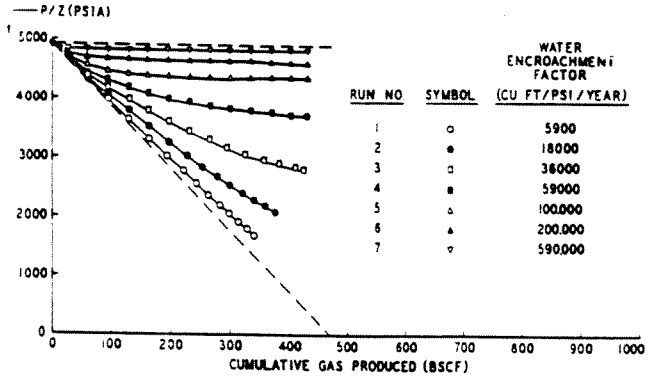

Fig. 2—Curves of p/z for gas reservoirs with water influx. Schilthuis method.

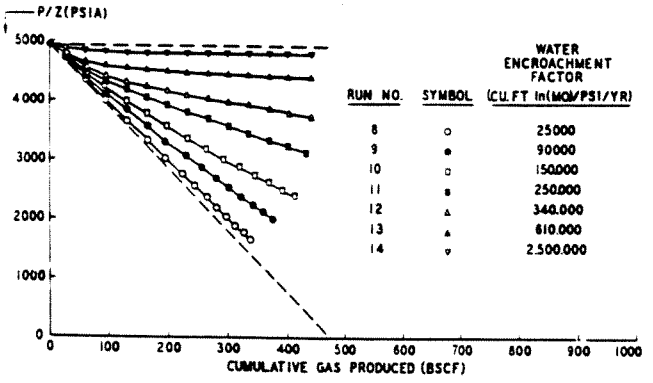

Fig. 3—Curves of p/z for gas reservoirs with water influx. Hurst simplified method.

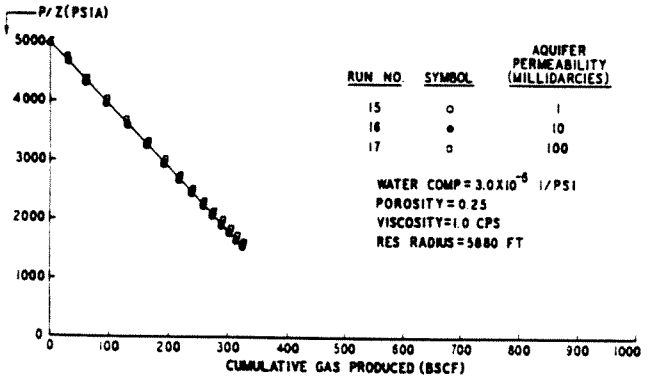

Fig. 4—Curves of p/z for gas reservoirs with water influx. van Everdingen-Hurst, finite, $R_e/R_r = 1.5$.

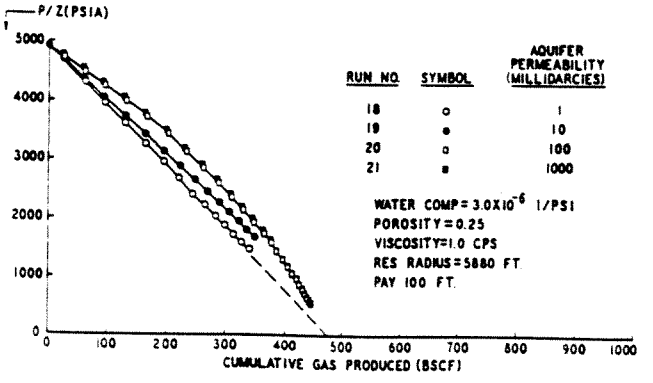

Fig. 5—Curves of p/z for gas reservoirs with water influx. van Everdingen-Hurst method, finite, $R_e/R_r = 5$.

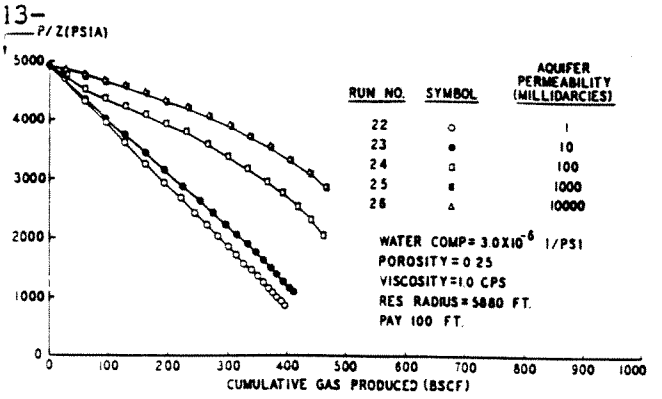

Fig. 6—Curves of p/z for gas reservoirs with water influx, van Everdingen-Hurst method, finite, $R_e/R_r = 10$.

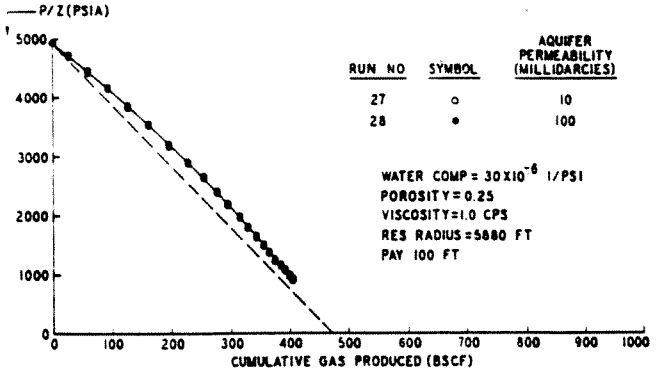

Fig. 7—Curves of p/z for gas reservoirs with water influx, van Everdingen-Hurst method, finite, $R_e/R_r = 1.5$.

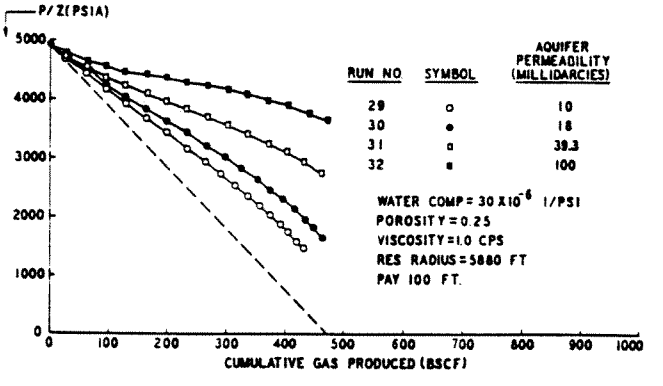

Fig. 8—Curves of p/z for gas reservoirs with water influx, van Everdingen-Hurst method, finite, $R_e/R_r = 5$.

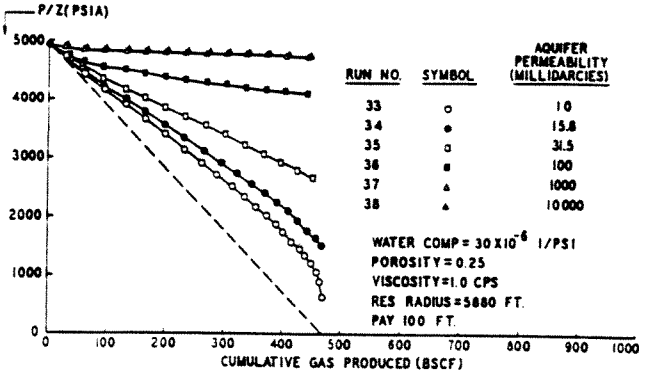

Fig. 9—Curves of p/z for gas reservoirs with water influx. van Everdingen-Hurst method, finite, $R_e/R_r = 10$.

the effect of the aquifer is negligible for a given water compressibility regardless of the permeability (Fig. 4). However, for a higher water compressibility an effect is felt for comparable mobilities (Fig. 7).

In general the pressure is maintained at higher levels as the water compressibility, aquifer size or water mobility is increased. Yet, even with increases in mobility an extreme curve was approached for the closed aquifers (Runs 25 and 26, Fig. 6). In these cases pressure drops in the aquifer were small and the shapes were controlled by the water compressibilities.

Conclusions

Fig. 10 illustrates the increasing error that occurs if a p/z curve is extrapolated with no regard for water encroachment. As the relative size of the aquifer increases from $R_e/R_r = 1.5$ to 10, the error increases from a negligible amount to an estimate of over 100 per cent of the actual initial gas in place. This estimate would be made after 65 per cent of the initial gas in place is produced.

This leads to the principal conclusion that it is dangerous to extrapolate p/z charts on a straight line without considering the possibility of water influx.

Runs performed here eliminated measurement error and the curved portions were produced under realistic production schedules. Thus, curved portions at the start of production history can be caused by the unsteady-state nature of the aquifer and not solely by measurement errors. So, these curved portions should not be neglected, but ought to be regarded as an indication of possible water encroachment.

These results make a case for accelerated early production so that the inflections will be accentuated, permitting better early estimates of gas in place.

Acknowledgment

The authors thank the Phillips Petroleum Co. for permission to publish this work. Special thanks are due R. V. Smith for his cooperation and assistance.

References

1. Schilthuis, R. J.: "Active Oil and Reservoir Energy", *Trans.*, AIME (1936) **118**, 33.
2. van Everdingen, A. F. and Hurst, W.: "The Application of the Laplace Transformation to Flow Problems in Reservoirs", *Trans.*, AIME (1949) **186**, 305.
3. Hurst, W.: "Water Influx Into a Reservoir and Its Application to the Equation of Volumetric Balance", *Trans.*, AIME (1943) **151**, 57.
4. van Everdingen, A. F., Timmerman, E. H. and McMahon, J. J.: "Application of the Material Balance Equation to a Partial Water Drive Reservoir", *Trans.*, AIME (1953) **198**, 51.
5. Pirson, S. J.: *Oil Reservoir Engineering*, 2nd Ed. McGraw-Hill Book Co., Inc., New York (1958) 608.
6. Stanley, L. T.: "Curve-Fitting Cuts Material Balance Calculations", *Pet. Eng.* (Aug., 1961) 90.
7. Hubbard, R. M. and Elenbaas, J. R.: "Determining Gas-Filled Pore Volume in a Water-Drive Gas Storage Reservoir", *Jour. Pet. Tech.* (April, 1964) 383.
8. Frick, T. C.: *Petroleum Production Handbook*, Vol. II, McGraw-Hill Book Co., Inc., New York (1962) 30.
9. Cullender, M. H. and Smith, R. V.: "Practical Solution of Gas-Flow Equations for Wells and Pipelines with Large Temperature Gradients", *Trans.*, AIME (1956) **207**, 281.

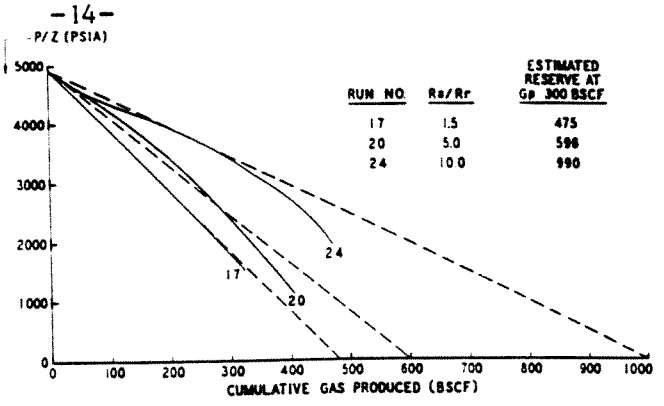

Fig. 10—Comparison of p/z curves for increasing aquifer sizes, van Everdingen-Hurst, radial finite.

APPENDIX A

Derivation of the Basic Equations

The apparent reserves for a gas field are those determined when no water encroachment is assumed, or,

$$V_p = V_{pi} \quad \ldots\ldots\ldots\ldots \quad (A\text{-}1)$$

where V_{pi} is the original pore volume, cu ft.

V_p is the pore volume containing gas at some later time.

$$V_p = (G_a - G_p)B_g \quad \ldots\ldots\ldots \quad (A\text{-}2)$$

$$V_{pi} = G_a B_{gi} \quad \ldots\ldots\ldots\ldots \quad (A\text{-}3)$$

where G_a = the apparent original gas in place, scf
G_p = cumulative gas produced, scf

B_{gi} and B_g are the gas formation volume factors, cu ft/scf.

$$B_{gi} = \frac{p_{sc} T_i Z_i}{p_i T_{sc}} \quad \ldots\ldots\ldots\ldots \quad (A\text{-}4)$$

$$B_g = \frac{p_{sc} T z}{p T_{sc}} \quad \ldots\ldots\ldots\ldots \quad (A\text{-}5)$$

Substituting Eqs. A-2 and A-3 into Eq. A-1 and solving for G_a gives

$$G_a = G_p\left(\frac{B_g}{B_g - B_{gi}}\right) \quad \ldots\ldots\ldots \quad (A\text{-}6)$$

When water encroachment is considered, Eq. A-1 is replaced by

$$V_p = V_{pi} - W_e \quad \ldots\ldots\ldots\ldots \quad (A\text{-}7)$$

to account for the water influx W_e.

Under these conditions, G_a in Eqs. A-2 and A-3 is defined as G_r (real initial in place gas), or,

$$V_p = (G_r - G_p)B_g \quad \ldots\ldots\ldots \quad (A\text{-}8)$$

and

$$V_{pi} = G_r B_{gi} \quad \ldots\ldots\ldots\ldots \quad (A\text{-}9)$$

Substitution of Eqs. A-8, A-9, and

$$W_e = K_r S(p,t) \quad \ldots\ldots\ldots\ldots \quad (A\text{-}10)$$

into Eq. A-7 gives

$$G_r = \frac{G_p B_g}{(B_g - B_{gi})} - \frac{K_r S(p,t)}{(B_g - B_{gi})} \quad \ldots \quad (A\text{-}11)$$

where K_r is the water encroachment factor and $S(p,t)$

TABLE 4

R_n/R_r	Middle Range of Δtd_i From	To	Equation B-10—A Constants A_1	A_2	A_3	A_4	A_5	Stabilized State Values Above the Middle Range
1.5	.1206	0.7	− 0.03255975	−0.02485001	0.03179695	0.007970778	0.6164517	0.6235899
2.0	.418	2.5	0.3852062	−0.09626595	−0.05244533	−0.004754153	1.281475	1.509915
2.5	.815	6.0	0.7919653	0.05396428	−0.06348801	−0.01234595	1.534877	2.634689
3.0	1.33	11.0	1.046089	0.2388103	−0.08575203	−0.008445356	1.574667	3.994681
3.5	1.12	25.0	0.4178854	1.292179	−0.4404957	0.03704949	1.630682	5.650575
4.0	2.05	34.0	− 2.231692	3.177286	−0.8411667	0.06444676	2.779082	7.499222
4.5	2.62	46.0	− 6.108747	5.413047	−1.266439	0.09235701	4.890919	9.619498
5.0	3.06	60.0	− 6.429505	4.823608	−0.8503674	0.03632684	5.599367	11.97866
6.0	5.85	110.0	−24.90336	12.44925	−2.042113	0.1044283	20.58242	17.48006
7.0	8.48	160.0	−43.33130	17.84979	−2.486980	0.1043855	39.95260	23.95055
8.0	9.29	240.0	−51.48727	19.26185	−2.365595	0.08228036	50.46776	31.66351
9.0	9.96	280.0	−31.97360	8.612722	−0.05276312	−0.08174990	38.52328	39.96676
10.0	14.52	360.0	−20.55106	0.6903652	1.759464	−0.2079732	37.02682	49.14654

is a function of pressure and time and describes the unsteady-state water influx.

Subtraction of Eq. A-11 from Eq. A-6 results in the basic equation

$$G_n = G_r + \frac{K_r S(p,t)}{(B_n - B_{n-1})} \quad \ldots\ldots\ldots \quad \text{(A-12)}$$

APPENDIX B

Definition of $S(p,t)$

Schilthuis Method

$$S(p,t) = \sum_{i=2}^{n} \Delta p_i \, \Delta t_i \quad \ldots\ldots\ldots \quad \text{(B-1)}$$

$$\text{where } \Delta p_i = p_i - \frac{(p_i + p_{i-1})}{2} \quad \ldots\ldots\ldots \quad \text{(B-2)}$$

$$\text{and } \Delta t_i = t_i - t_{i-1} \quad \ldots\ldots\ldots \quad \text{(B-3)}$$

where n = number of pressure points
t_i = time in years
p = aquifer pressure (inner boundary) psia.

Hurst-Simplified Method

$$S(p,t) = \sum_{i=2}^{n} \frac{\Delta p_i \, \Delta t_i}{\ln(12 t_i)} \quad \ldots\ldots\ldots \quad \text{(B-4)}$$

where Δp_i and Δt_i are still defined by Eqs. B-2 and B-3

van Everdingen-Hurst Method

$$S(p,t) = \sum_{i=1}^{n-1} \Delta p_i \, q_{\Delta t_{di}} \quad \ldots\ldots\ldots \quad \text{(B-5)}$$

where

$$\Delta p_i = \frac{p_{i+1} - p_i}{2} \quad \ldots\ldots\ldots \quad \text{(B-6)}$$

for $i = 1$, and

$$\Delta p_i = \frac{p_{i+1} - p_{i-1}}{2} \quad \ldots\ldots\ldots \quad \text{(B-7)}$$

for $i = 2$ to $n - 1$.

$q\Delta t_{di}$ is the dimensionless flow rate and is a function of Δt_{di} (the dimensionless time increment) and aquifer geometry.

$$\Delta t_{di} = 2.309 \left(\frac{k \quad \Delta t}{\phi \mu C_w (R_r)^2} \right), \quad \ldots\ldots \quad \text{(B-8)}$$

with k in millidarcies, t in years, ϕ a fraction, μ in cp, C_w in 1/psi, R_r in ft.

$q\Delta t_{di}$ is defined under the following conditions. All $\Delta t_{di} < 0.01$, or the linear system

$$q\Delta t_{di} = 2\sqrt{\Delta td_i/\pi}. \quad \ldots\ldots\ldots \quad \text{(B-9)}$$

Infinite Radial System

$$(0.01 < \Delta t_{di} \leq 10^4)$$

$$q\Delta t_{di} = e^{(A_1 \ln \Delta t_{di} - A_2) \ln \Delta t_{di} + A_3 (\ln \Delta t_{di})^2 - A_4 (\ln \Delta t_{di})^3 + A_5}$$

where $A_1 = 0.647692$

$A_2 = 0.0177318$

$A_3 = -0.0002737391$

$A_4 = -0.4318125 \times 10^{-4}$

$A_5 = 0.4506432.$

Finite Radial Systems

The finite radial systems are defined by the infinite radial Eq. B-10, where $\Delta t_{di} > 0.01$ and less than the middle range defined in Table 4. In the middle range the dimensionless flow is defined by an equation of the same form as Eq. B-10, but with constants shown in Table 4. Table 4 also gives the steady-state values applicable above the middle range. ★★★

J. R. BRUNS *(left) is a senior mathematical engineer in the Phillips Petroleum Co.'s Computing Dept. For the past seven years he has worked in reservoir engineering computer applications. He has a BS in chemical engineering from the U. of Missouri, an MS in chemical engineering from Illinois Institute of Technology, and a Master of Gas Technology degree from the Institute of Gas Technology.* M. J. FETKOVICH *(right) is a reservoir engineering and gas technology analyst in the Reservoir and Production Project Group of Phillips. He graduated from the U. of Pittsburgh in 1954 with a BS degree in petroleum and natural gas engineering and soon joined Phillips.* V. C. MIETZEN *(center) is a senior electronic computer programmer for Phillips at Bartlesville, Okla. He joined Phillips after receiving his BS degree in petroleum engineering from The U. of Texas in 1960. He worked as a staff engineer in the Pauls Valley, Okla., Area Office before joining the Computer Dept. in 1963.*